*Original Article*

# Use of Radioiodinated Peptide Arg-Arg-Leu Targeted to Neovascularization as well as Tumor Cells in Molecular Tumor Imaging

Xia Lu[1, 2, 3], Ping Yan[1], Rong-fu Wang[1*], Meng Liu[1], Ming-ming Yu[4], Chun-li Zhang[1]

[1]*Department of Nuclear Medicine, Peking University First Hospital, Beijing 100034, China*
[2]*Radiology Center, Beijing Aerospace General Hospital, Beijing 100076, China*
[3]*Key Laboratory of Radiopharmaceuticals (Ministry of Education), College of Chemistry, Beijing Normal University, Beijing 100191, China*
[4]*Department of Nuclear Medicine, Clinical Medical College, Yangzhou University, Yangzhou 225000, China*

**DOI: 10.1007/s11670-012-0052-8**


**ABSTRACT**

**Objective:** To explore a tumor peptide imaging agent Arginine-Arginine-Leucine (Tyr-Cys-Gly-Gly-**Arg**-**Arg**-**Leu**-Gly-Gly-Cys, tripeptide RRL [tRRL]) that targeted to tumor cells and tumor-derived endothelial cells (TDECs) and primarily investigate the possible relationship between tRRL and vascular endothelial growth factor receptor 2 (VEGFR-2).

**Methods:** The tRRL sequence motif was identified as a tumor molecular marker specifically binding to TDECs. Tyrosine was conjugated to the amino terminal of RRL (Cys-Gly-Gly-**Arg**-**Arg**-**Leu**-Gly-Gly-Cys) for labeling with radionuclide iodine-131 ($^{131}$I-tRRL). The uptake ability and molecular binding of tRRL to tumor cells and angiogenic endothelium were studied using flow cytometry and radioactivity counter *in vitro*. Whether VEGFR-2 is the binging site of tRRL was investigated. Biodistribution and single-photon emission computed tomography (SPECT) imaging of $^{131}$I-tRRL were used to evaluate the effectiveness of this new imaging agent to visualize varied tumor xenografts in nude mice.

**Results:** *In vitro* cellular uptake experiments revealed that tRRL could not only adhere to tumor angiogenic endothelial cells but also largely accumulate in malignant tumor cells. VEGFR-2, which is highly expressed on TDECs, was probably not the solely binding ligand for tRRL targeted to tumor angiogenic endothelium. $^{131}$I-tRRL mainly accumulated in tumors *in vivo*, not other organs at 24 h after injection. SPECT imaging with $^{131}$I-tRRL clearly visualized tumors in nude mice, especially at 24 h.

**Conclusion:** Radioiodinated tRRL offers a noninvasive nuclear imaging method for functional molecular imaging of tumors targeted to neovascularization, and may be a promising candidate for tumor radioimmunotherapeutic carrier.

**Key words:** Iodine-131; Peptide **Arg-Arg-Leu** (tRRL); Uptake ability; Molecular tumor imaging

## INTRODUCTION

Solid malignant tumors are mainly composed of tumor cells and tumor vascular endothelium by which metabolites are transported to allow tumor cells to survive and initiate the metastases of tumors[1, 2]. Imaging techniques, including modern nuclear medicine such as positron emission computed tomography (PET), play important roles in tumor clinical diagnosis and treatment. Recently, molecular imaging, especially single-photon emission computed tomography (SPECT) imaging, is being used to explore new areas[3].

Despite the progress in research into cancer diagnosis and treatment, limitations of imaging methods with good sensitivity and specificity of imaging agents used in the clinic are still challenging. Because angiogenesis is an essential step for tumor

**Received** 2011–06–25; **Accepted** 2011–10–18
This work was supported by grants from the National Natural Science Foundation of China (NSFC 30870729, 81071183/H1806 and 30900374), National "973" Basic Research Program of China (No. 2006CB705705-1), National Education Ministry 985 Project of China (985-2-056) and Research Fund for the Doctoral Program of Higher Education of China (200800011061).
* Corresponding author.
E-mail: rongfu_wang2003@yahoo.com.cn

growth and initiation of metastasis[4], researchers have devoted enormous energy to the discovery of angiogenic factors[5, 6] and developed angiogenesis imaging methods for early diagnosis, optimal treatment for individual patients and predicting subsequent clinical response[7-11]. To meet the demand for rapid development and potential clinical application of anti-angiogenesis tumor therapy, developing noninvasive imaging methods with a targeted imaging agent specifically binding with tumor vascular endothelial cells is desirable.

Radiolabeled peptides attract increasing interest in imaging angiogenesis and targeted radiotherapy of malignant tumors[12–16]. These small-molecule agents could gain access to target sites more easily than monoclonal antibodies[17]. Special emphasis has been devoted to the development of peptides labeled with radionuclides. Ruoslahti and others identified various peptides with binding specificity to angiogenic endothelium and endothelial cells from various organs[18, 19]. Brown, et al. identified the nonapeptide sequence motif Cys-Gly-Gly-**Arg-Arg-Leu**-Gly-Gly-Cys (RRL) with binding specificity for tumor-derived endothelial cells (TDECs) by use of FliTrx™[20]. Further ultrasonic imaging after microbubbles conjugated RRL (MB-RRL) injection showed that ultrasonography of tumors was enhanced with MB-RRL[21]. Other researchers conjugated 2 near-infrared dyes (Alexa 680, 800) to RRL peptide and found injected tumor but not any other site or organ with an appreciable image signal in human PC3 prostate tumor-bearing mice or transgenic mice with prostate cancer[22]. In our previous study, we designed and synthesized decapeptide tRRL[23].

In this study, we explored the association of tRRL to tumor cells and TDECs and the possible relationship between tRRL and vascular endothelial growth factor receptor 2 (VEGFR-2). We aimed to develop a molecular imaging agent with high sensitivity and specificity to visualize tumors *in vivo* for a potential carrier for radioimmunotherapy.

## MATERIALS AND METHODS

### Peptide Design and Synthesis

The sequence of tRRL was redesigned and synthesized as described previously[23]. Tyrosine was added to the amino terminus of RRL and labeled by iodine-131. The new sequence was (Tyr)-Cys-Gly-Gly-**Arg-Arg-Leu**-Gly-Gly-Cys (tRRL), and the control peptide sequence was (Tyr)-Cys-Gly-Gly-Gly-Gly-Gly-Gly-Gly-Cys (tGGG). One part of the synthetic tRRL compounds was conjugated with fluorescein isothiocyanate (FITC) during synthesis. The lyophilized peptide was stored at –20°C.

### Radiolabeling with Iodine-131

Decapeptide tRRL was labeled with $^{131}$I by electrophilic radioiodination by use of chloramine-T as oxidizing agent, essentially as described previously[23]. Briefly, 50 μg tRRL was labeled with 37 MBq [$^{131}$I]Na. After a 2-min reaction, the mixture was diluted with phosphate-buffered saline (PBS) containing 0.1% bovine serum albumin and purified by a size-exclusion chromatography column (Sephadex G-10 M). The $^{131}$I peak eluting from the column was collected, and radioactivity was measured.

### *In Vitro* Studies

#### *Cell Lines and Regents*

HepG2 (human hepatocellular liver carcinoma cell line), B16 (mouse melanoma cell line), SKOV3 (human ovarian carcinoma cell line), EOMA (mouse endothelioma cell line) (10th passage), HK-2 (immortalized proximal tubule epithelial cell line) (17th to 19th passage), and human umbilical vein endothelial cells (HUVECs) from the American Type Culture Collection were maintained as recommended. THP-1 cells (human acute monocytic leukemia cell line) (10th passage) and human aortic endothelial cells (HAECs) (2nd to 5th passage) were gifts from Professor Chun-yan Zhou (Peking University Health Science Center, Department of Biochemistry and Molecular Biology, Beijing, China). EOMA, HUVECs and HAECs were cultured in extracellular matrix medium containing 5% fetal bovine serum (SclenCell), 100 μg/ml streptomycin, 100 U/ml penicillin, and 1% endothelial cell growth supplement (SclenCell). HepG2, THP-1 and HK-2 cells were maintained in DMEM/High Glucose medium containing 10% fetal bovine serum (GIBCO), 2 mmol/L glutamine, and 4,500 mg/L glucose. SKOV3 and B16 cells were maintained in RPMI-1640 medium supplemented with 10% fetal bovine serum and 1 mmol/L glutamine. All commercially available chemical reagents were used without further purification. In each independent experiment, HUVECs were used before the fifth passage. All cells were incubated at 37°C in a humidified atmosphere containing 5% $CO_2$. The experiments were performed with cells in the logarithmic phase of growth.

#### *$^{131}$I-tRRL Binding Experiment*

HUVECs and B16, HepG2 and HK-2 cells were cultured in 24-well plates ($5\times10^4$ per well). Cells were starved for 16 h in serum-free medium, then cocultured with medium containing 37 kBq $^{131}$I-tRRL per well. We harvested the medium (non-uptake

$^{131}$I-tRRL) and cells (uptake $^{131}$I-tRRL) of each well at 0.5, 1, 2, 4, 6, and 24 h, and radioactivity was measured by use of a γ-well counter along with a standard (treatment for each well repeated 3 times). The binding ability of $^{131}$I-tRRL was represented by the ratio of mean uptake. Uptake ratio = uptake counts / mean total counts (uptake and non-uptake counts) ×100%.

### *Flow Cytometry*

HUVECs, and B16 and HK-2 cells were cultured in appropriate medium and incubated with FITC-tRRL (2 μg/ml) for different times after being starved for 16 h in serum-free medium. The cells were then harvested and re-suspended in PBS at $2\times10^5$ cells/ml for flow cytometry analysis. The same number of cells in each cell line was measured to assess the uptake ability of FITC-RRL by using of a flow cytometer (BD FACSCalibur). A total of 15,000 gated cells were counted, and fluorescence intensity in each cell was determined by green fluorescence on binding tRRL to cells. The median fluorescence intensity was analyzed by use of CellQuest (Becton Dickinson).

### *RT-PCR*

All RNAs were isolated from $5\times10^5$/ml SKOV3s, HAECs and EOMAs after Trizol reagent (Invitrogen) digestion. The sequences of primers were as follows: VEGFR-2 (314 bp) forward, 5′-AGGCAGCTCACAG-TCCTAGAGC-3′, reverse, 5′-GTCTTTTCCTGGGCA-CCTTCTA-3′; GAPDH (internal control) (405 bp) forward, 5′-ACCCAGAAGACTGTGGATGG-3′, reverse, 5′-TTCTAGACGGCAGGTCAGGT-3′. All primers were purchased from AuGCT Biotechnology Synthesis Lab (Beijing, China). The expression of VEGFR-2 mRNA in each cell line was measured.

### *Western Blot Analysis*

Total protein of SKOV3, HAEC, EOMA and THP-1 cells and HUVECs was extracted by use of RIPA lysis buffer. Protein concentration was determined by use of a BCA protein assay kit. Samples were then separated on 6%−10% SDS-polyacrylamide gels and transferred to nitrocellulose (NC) membranes. The membranes were blotted with primary antibodies against VEGFR-2 (Abeam) and GAPDH (Santa Cruz Biotechnology, USA). Signals were visualized by horseradish peroxidase-conjugated secondary antibodies and enhanced chemiluminescence reagents.

### *In Vivo* Studies

### *Biodistribution*

All animal experiments complied with the Guidelines for the Care and Use of Research Animals established by Peking University Animal Studies Committee. BALb/c nu/nu mice [male, (20±3) g, 4 to 6 weeks old; Department of Laboratory Animal Science, Peking University Health Science Center, Beijing, China] were used in this study. The mice were injected with $1\times10^7$ B16 cells in the left upper limbs, and the tumors were allowed to grow to a diameter of 0.8 cm. Five BALb/c nu/nu mice with melanoma xenografts were injected with 37 kBq $^{131}$I-tRRL in 200 μl of saline via the tail vein. After 24 h, 5 mice were sacrificed by cervical dislocation, and 100 μl blood samples were collected. Tissues of interest (heart, lung, liver, stomach, spleen, small intestine, kidney, bladder, bone marrow, skeletal muscle and tumor) were removed and weighed. Radioactivity of all tissues was measured by use of a NaI (T1) well counter. Biodistribution results were recorded as percentage of injected dose per gram (%ID/g).

### *SPECT Imaging*

BALb/c nu/nu mice were randomly divided into 2 groups of 5 mice each, as the melanoma group and hepatic carcinoma group (for injection of $^{131}$I-tRRL). The tumor cells of B16 and HepG2 ($1\times10^7$ cells) were injected subcutaneously in the left upper limbs of each mouse. When the diameter of tumor reached about 0.8 cm, tumor-bearing mice underwent imaging. The mice received 400 mg sodium perchlorate over 3 d for thyroid blockage. Then the mice were injected with $^{131}$I-tRRL (7.4 MBq) via the tail vein. All injections were tolerated well. At 24 h after injection, whole-body gamma camera imaging was performed in B16 and HepG2 xenografts in the Department of Nuclear Medicine, Peking University First Hospital, by SPECT (SPR SPECT; GE Healthcare, Inc.) equipped with a low-energy, high-resolution, and parallel-hole collimator. Static images (100,000 counts) obtained with a zoom factor of 2.0 were digitally stored in a 256×256 matrix.

### Statistical Analysis

The variables are expressed as $\bar{x}\pm s$. Statistical comparisons of variables were performed by 1-way ANOVA analysis, and $P$ values of less than 0.05 were considered statistically significant.

## RESULTS

### Small Peptide Conjugation and Radiolabeling

The tRRL peptide was radiolabeled with $^{131}$I under optimal conditions ($^{131}$I-tRRL). Under the set of conditions, average labeling efficiencies of 60%±5% ($n$=5) were achieved within 2-minute reaction at room temperature by chloramine-T, specific activities of up

to 1,850 kBq/mg were obtained, and radiochemical purity was >95% after purification. Figure 1 shows the elution curve with chromatography on a Sephadex G-10 column. The first radioactive peak in Figure 1A corresponded to the ultraviolet (UV) absorbance peak in Figure 1B, which was the pure $^{131}$I-tRRL. Therefore, the first radioactive peak was $^{131}$I-tRRL and the second peak was unlabeled iodine 131 in Figure 1A.

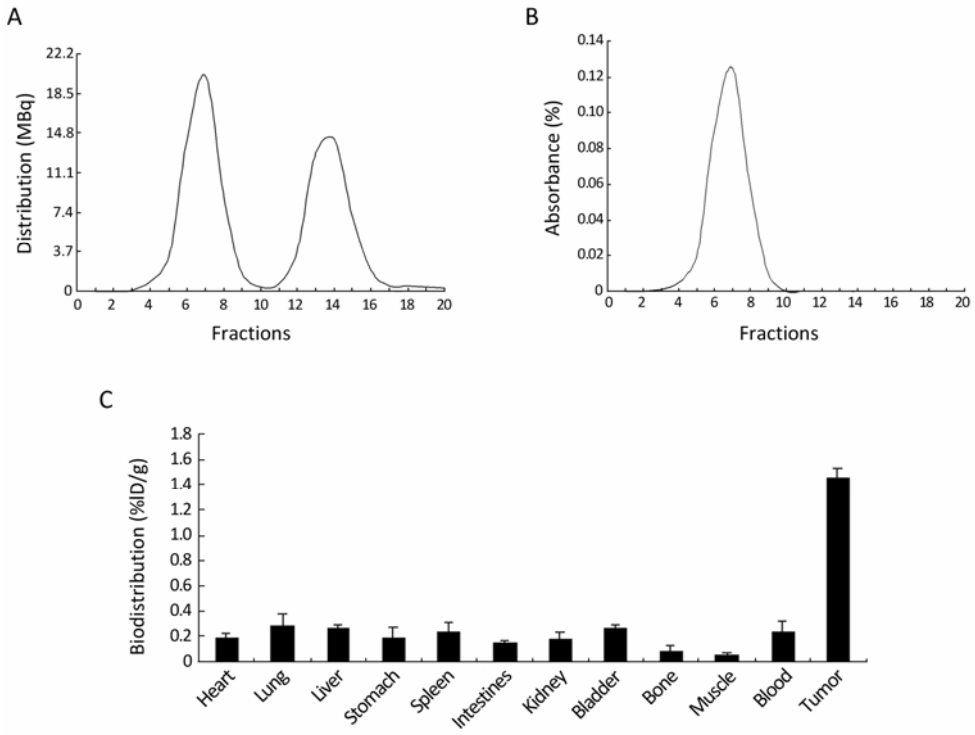


**Figure 1.** The elution curve from Sephadex G-10 gel filtration column (1–20 cm) purified radio-iodinated product. **A:** The distribution of $^{131}$I-tRRL in each pipe. Elute rate: 0.5 ml/min, 2 min/fraction. The first peak was $^{131}$I-tRRL and the second peak was unlabeled $^{131}$I. **B:** 280 nm UV absorbance of eluted fractions confirmed that the first peak was pure $^{131}$I-labeled tRRL peptide. **C:** Biodistribution (%ID/g) of $^{131}$I-labeled tRRL peptide at 24 h, after injection in melanoma-bearing BALb/c nude mice ($n$=5). $^{131}$I-tRRL was mainly accumulated in tumor and other organs showed background uptake.

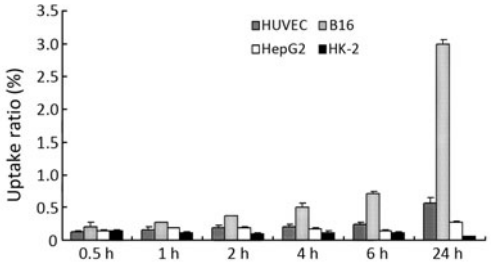


**Figure 2.** Uptake of $^{131}$I-tRRL by HUVECs, B16, HepG2 and HK-2 cells. For HUVECs, and HepG2, B16 cells, the uptake ratio was increased with prolonged incubated time. Conversely, the uptake ratio of $^{131}$I-tRRL in HK-2 cells was lower at every time and slightly decreased at 24 h. B16 cells had highest uptake of $^{131}$I-tRRL at each time point especially at 24 h.

### Biodistribution of the Probe in Mouse

The biodistribution of $^{131}$I-tRRL was measured in melanoma xenograft-bearing nude mice after intravenous injection of the probe for 24 h (Figure 1C). The probe was cleared quickly from heart, liver, stomach, spleen, intestinal tract, kidney, bladder, bone, muscle and blood, and little radioactivity existed in lung. $^{131}$I-tRRL was significantly accumulated in the tumor, and the uptake was (1.45±0.09) %ID/g ($n$=5, $P$<0.05), a higher level than that in the other organs.

### Uptake of $^{131}$I-tRRL by Tumor and Non-tumor Cells

We cultured HUVECs and HepG2, B16 and HK-2 cells in 500 μl medium with 37 kBq $^{131}$I-tRRL and FITC-tRRL (2 μg/ml) for different times and measured the radioactivity and fluorescence intensity in cells and in media to calculate the uptake ratio of $^{131}$I-tRRL by the cells. For HUVECs, HepG2 and B16 cells, the uptake ratio was increased with prolonged incubated time (Figures 2, 3). Conversely, the uptake ratio of $^{131}$I-tRRL in HK-2 cells was low at every time point and slightly decreased at 24 h. After incubation for 24 h, the uptake ratio of $^{131}$I-tRRL was significantly higher in B16, HepG2 cells and HUVECs. The binding ability of tRRL to B16 was about 50 times higher than that to HK-2 cells ($P$<0.05) and 5 times higher than that to HUVECs ($P$<0.05).

### γ-Camera Scintigraphy

Standard techniques were used for recording and visualization. Serial whole-body static images were

obtained at 24 h after $^{131}$I-tRRL injection via the tail vein on melanoma and liver cancer xenografts in BALb/c nude mice. The mean radioactivity in the whole body decreased gradually. Most tumors were clearly visualized at 24 h. Targeted tRRL indicated the specific accumulation in prostate carcinoma and also melanoma and liver cancer *in vivo* (Figure 4).

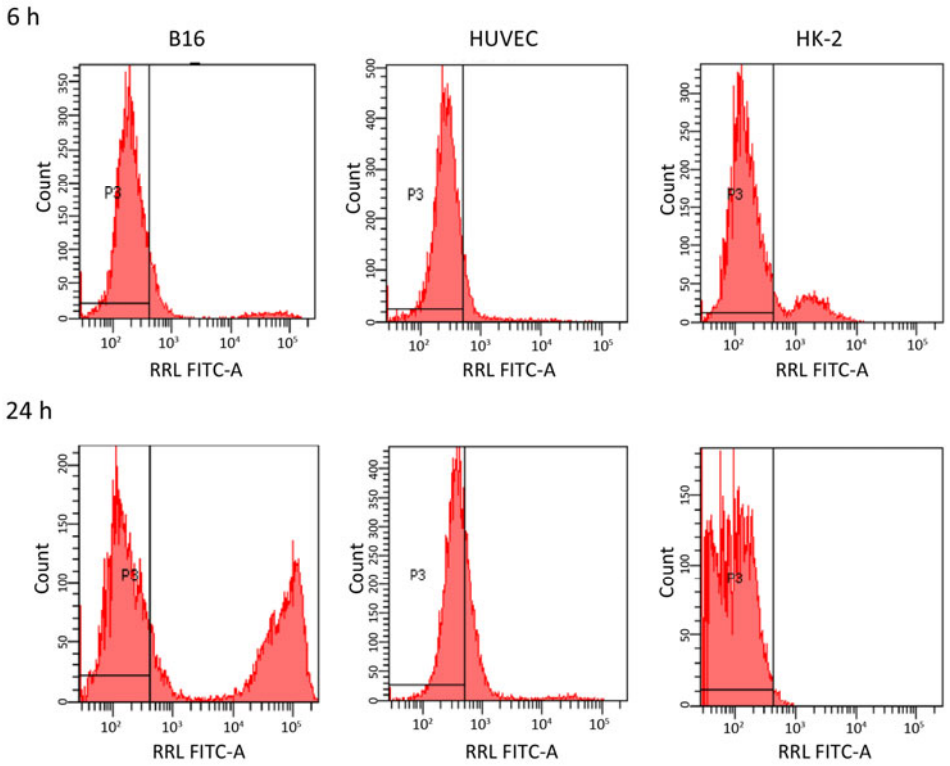


**Figure 3.** Binding of FITC-tRRL probe in HUVECs and in B16 and HK-2 cells measured by FCM. After counting 15,000 cells in each cell lines, the fluorescence intensity of each cell was measured to assess the binding ability of tRRL to different cell lines. At 24 h after incubation, the amount of FITC-tRRL binding to B16 cells was significantly increased than that in HUVECs, which was almost negative in HK-2 cells.

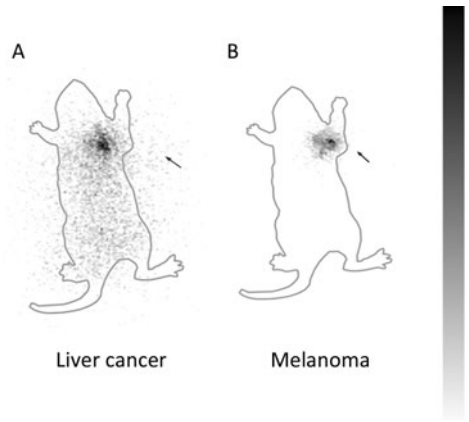


**Figure 4.** γ-camera scintigraphy of nude mice bearing human liver cancer (A) and melanoma (B). Planar γ-camera images were collected 24 h after administration of imaging probe $^{131}$I-tRRL. Tumor (arrow) was clearly visualized.

### Association of VEGFR-2 Expression and Staining of FITC-tRRL in Tumor Cells

VEGFR-2 (kinase insert domain receptor) is a subtype of receptors for VEGF, which plays a key role in endothelial proliferation and vascular development. We therefore examined whether tRRL targeted to HUVECs and tumor cells by combining with VEGFR-2 for imaging capability in tumor angiogenesis. RT-PCR and Western blotting analysis revealed high expression of VEGFR-2 in EOMA cells and HUVECs, weak expression in HAEC cells, and absent expression in SKOV3 cells and THP-1 cells (Figure 5A and B). The results of cell binding experiment with FITC-tRRL showed that SKOV3 cells with absent expression of VEGFR-2 had high uptake of FITC-tRRL (Figure 5C). Therefore, it seems that VEGFR-2 had no consistent association with the peptide tRRL.

## DISCUSSION

We tried to conjugate tyrosine to the amino terminal of RRL and GGG, which could be labeled with $^{131}$I by the chloramine-T method. The purity of compounds was more than 99% and identified by high performance liquid chromatography (HPLC) (Scilight Biotechnology LLC., Beijing). A mean labeling efficiency of 60%±5% was achieved within 2 minutes at room temperature, and radiochemical purity was >95% after purification. In our previous study, the

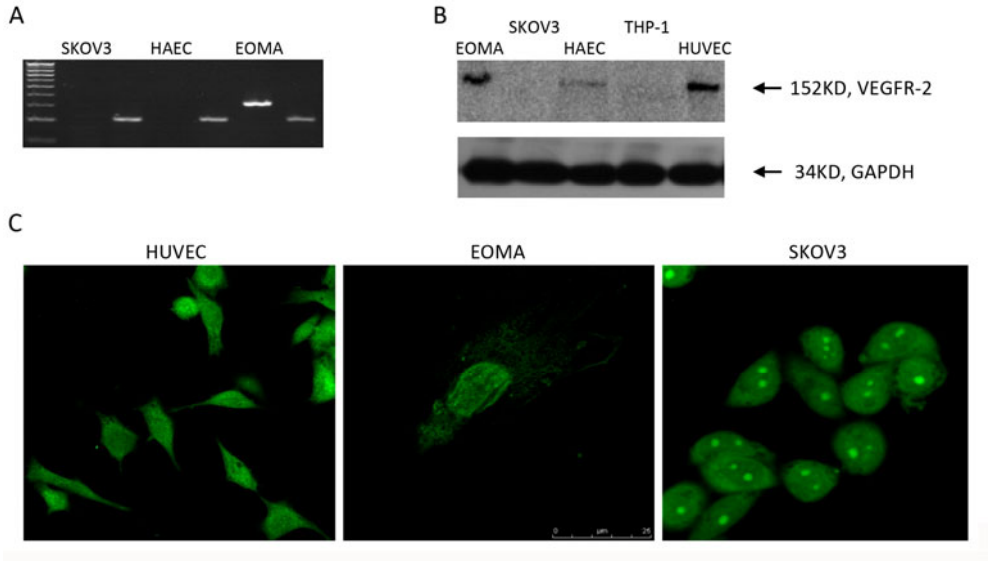


**Figure 5.** Expression of VEGFR-2 and FITC-tRRL in different cell lines. **A:** RT-PCR analysis of mRNA expression of VEGFR-2 in SKOV3 cells, HAECs and EOMA cells with GAPDH as an internal control. **B:** Western blot analysis of the protein expression of VEGFR-2 in EOMA and SKOV3 cells, HAECs, THP-1 cells and HUVECs with GAPDH as an internal control. **C:** Fluorescence staining indicated the location of tRRL. FITC-tRRL was taken up by HUVECs and EOMA and SKOV3 cells (green, 2 μg/ml).

biodistribution of $^{131}$I-tRRL and $^{131}$I-tGGG was measured at different times in PC3 xenograft-bearing nude mice. At 1 hour after injection, the probe accumulated primarily in blood, stomach, kidney, liver, spleen and intestinal tract, and moderately in the tumor. At 6 hours after injection, the probe level was decreased in these normal tissues but was increased slightly in the tumors. At 24 hours after injection, the probe level decreased further in these tissues and in the tumor, and the uptake was (0.65±0.12) %ID/g. In contrast, the level of $^{131}$I-tGGG peptide as the control probe accumulated less in these tissues and the tumor at 1 hour after injection. The level of the control probe decreased significantly at 6 and 24 hours after injection. It was only (0.06±0.04) %ID/g in tumors of $^{131}$I-tGGG at 24 hours after injection. $^{131}$I-tRRL but not control peptides could accumulate in tumors at 24 hours in prostate carcinoma xenografts. $^{131}$I-labeled tRRL peptide was stable *in vitro* and in the human body[21,23]. In our present distribution experiment, the uptake of $^{131}$I-tRRL in the tumor was up to (1.45±0.12) %ID/g at 24 hours after injection in melanoma xenografts. So tRRL could be radioiodinated, had a favorable uptake in tumors and could be used for imaging tumor angiogenesis, which agrees with previous reports.

Our present results showed that the amount of small-peptide tRRL could also combine predominantly with tumor cells besides adhering to TDECs. This phenomenon was firstly observed in the SKOV3 cell line and indicated that tumor cells had interaction with tRRL. Then cell binding experiments and flow cytometry analysis with $^{131}$I-tRRL, which could count the same number cells with each cell lines to avoid bias from cell numbers, were carried out. We confirmed that tumor cells could uptake tRRL by qualitative and quantitative measurements. This finding expanded the prediction of tRRL as a tumor angiogenesis agent[21]. In the past report, the binding properties of $^{123}$I-labeled $VEGF_{165}$ ($^{123}$I-$VEGF_{165}$) and $^{123}$I-$VEGF_{121}$ to HUVECs, several human tumor cell lines (HMC-1, A431, KU812, U937, HEP-1, HEPG2, HEP-3B and Raji), a variety of primary human tumors and some adjacent non-neoplastic tissues as well as normal human peripheral blood cells *in vitro* were analyzed by many researchers. Two classes of high-affinity $^{123}$I-$VEGF_{165}$-binding site were found on the cell surface of HUVECs. In contrast, one class of high-affinity binding sites for $^{123}$I-$VEGF_{165}$ was found on HMC-1, A431, HEP-1, HEP-G2, HEP-3B and U937 cells as well as many primary tumors. For $^{123}$I-$VEGF_{121}$, a single class of high affinity binding site was found on certain cell lines (HUVEC, HEP-1 and HMC-1) and distinct primary tumors (primary melanomas, ductal breast cancers and ovarian carcinomas as well as meningiomas). $^{123}$I-$VEGF_{165}$ and $^{123}$I-$VEGF_{121}$ had significantly greater specific binding to a variety of human tumor cells/tissues by VEGFR compared with the corresponding normal tissues or normal peripheral blood cells[24].

Tumor angiogenesis is a complex and coordinated process, requiring several signaling steps[25]. Besides human umbilical vein endothelial cells, some tumor cells were also found to express large numbers of VEGFRs[26]. VEGFR-2 is one of the major regulators of tumor angiogenesis, and activation of the VEGF/VEGFR-2 axis triggers multiple signaling pathways that result in endothelial cell survival, mitogenesis, migration, differentiation, and alterations

in vascular permeability[27]. Because of the important role of VEGFR-2 in tumor angiogenesis and high expression in TDECs[28], we analyzed the structure of possible candidate for tRRL including VEGFR-2, integrin $\alpha_v\beta_3$ and matrix metalloproteinases 2 (MMP-2). Finally we chose VEGFR-2 as a targeted site for tRRL as VEGFR-2 had relative lower dosing energy with tRRL calculated by V-life software, which means high affinity to tRRL in several candidate targeted sites. Moreover, the relationship between VEGFR-2 and tRRL attracted our attention since it was very important for the further research of tRRL in tumor angiogenesis. So we hypothesized that VEGFR-2 was the targeted site of tRRL binding to TDECs. However, the results showed that cell lines with distinguishing VEGFR-2 expression had universal uptake of tRRL. It seems that there are no consistent associational interactions between VEGFR-2 and tRRL in TDECs. The mechanism of tRRL binding to tumor cells and TDECs needs further study.

Targeting tumor cells is an advantage of tRRL over other tumor angiogenesis agents. The possible mechanisms of tRRL targeting tumor cells and tumor endothelial cells are as follows: (1) because tRRL was a small molecular weigh peptide and cancer cells were actively proliferating, the cells could uptake tRRL via the cell membrane, which shows the conjunction in cytoplasma and nuclei; (2) tRRL could combine with cancer cells by targeting to the nucleosome in various cancer cells, which showed one or two bright dots and demonstrated heavily stained nucleosomes; (3) tRRL was internalized by cancer cells via conjunction on the targeted receptor, which distributes in different membrane structures in cancer cells. How tRRL actually enters the membrane and locates in cells needs in-depth research.

Our present results also showed that $^{131}$I-tRRL was effective and reliable in detecting tumor lesions of not only prostate carcinoma but also other malignant tumors such as melanoma and liver cancer at 24 hours after injection in tumor-bearing mice. This result rapidly expands the use of $^{131}$I-tRRL in tumor molecular imaging. tRRL targeted TDECs and revealed tumor angiogenesis possibly through a special ligands expressed in TDECs. tRRL could combine with tumor cells as well as TDECs to reveal different malignant tumors. We are planning to further explore the relationship between tRRL and tumor cells and the mechanism of tRRL specially binding to TDECs.

These preliminary results demonstrated the efficiency of imaging tumors with $^{131}$I-tRRL. Our study highlighted and expanded the application of tRRL by our cell binding experiments and mechanism research. In this regard, the small peptide tRRL is useful and could be a potent targeted carrier for tumor radioimmunotherapy.

**Acknowledgment**

We thank Chun-yan Zhou (Peking University Health Science Center, Department of Biochemistry and Molecular Biology) for the generous gift of cell lines and Feng-qing Guo (Peking University First Hospital) for animal injection.

## REFERENCES

1. Glunde K, Pathak AP, Bhujwalla ZM. Molecular–functional imaging of cancer: to image and imagine. Trends Mol Med 2007; 13:287–97.
2. Gupta PB, Mani S, Yang J, et al. The evolving portrait of cancer metastasis. Cold Spring Harb Symp Quant Biol 2005; 70:291–7.
3. Wagner HN Jr. Advancing a molecular theory of disease. J Nucl Med 2008; 49:15N–34N.
4. Folkman J. Role of angiogenesis in tumor growth and metastasis. Semin Oncol 2002; 29(6 Suppl 16):15–8.
5. Aiello LP. Keeping in touch with angiogenesis. Nat Med 2000; 6:379–81.
6. Rosen L. Antiangiogenic strategies and agents in clinical trials. Oncologist 2000; 5(Suppl 1):20–7.
7. Davis DW, McConkey DJ, Abbruzzese JL, et al. Surrogate markers in antiangiogenesis clinical trials. Br J Cancer 2003; 89:8–14.
8. Costouros NG, Diehn FE, Libutti SK, et al. Molecular imaging of tumor angiogenesis. J Cell Biochem Suppl 2002; 39:72–8.
9. Anderson H, Price P, Blomley M, et al. Measuring changes in human tumour vasculature in response to therapy using functional imaging techniques. Br J Cancer 2001; 85:1085–93.
10. Padhani AR. Functional MRI for anticancer therapy assessment. Eur J Cancer 2002; 38:2116–27.
11. Miles KA. Functional computed tomography in oncology. Eur J Cancer 2002; 38:2079–84.
12. Heppeler A, Froidevaux S, Eberle AN, et al. Receptor targeting for tumor localisation and therapy with radiopeptides. Curr Med Chem 2000; 7:971–94.
13. Behr TM, Gotthardt M, Barth A, et al. Imaging tumors with peptide-based radioligands. Q J Nucl Med 2001; 45:189–200.
14. Breeman WA, de Jong M, Kwekkeboom DJ, et al. Somatostatin receptor mediated imaging and therapy: basic science, current knowledge, limitations and future perspectives. Eur J Nucl Med 2001; 28:1421–9.
15. Okarvi SM. Recent developments in $^{99m}$Tc-labelled peptide-based radiopharmaceuticals: an overview. Nucl Med Commun 1999; 20:1093–112.
16. Weiner RE, Thakur ML. Radiolabeled peptides in the diagnosis and therapy of oncological diseases. Appl Radiat Isot 2002; 57:749–63.
17. Foss CA, Mease RC, Fan H, et al. Radiolabeled small-molecule ligands for prostate-specific membrane antigen: *in vivo* imaging in experimental models of prostate cancer. Clin Cancer Res 2005; 11:4022–8.
18. Pasqualini R, Ruoslahti E. Organ targeting *in vivo* using phase display peptide libraries. Nature 1996; 380:364–6.
19. Rajotte D, Arap W, Hagedorn M, et al. Molecular heterogeneity of the vascular endothelium revealed by *in vivo* phage display. J Clin Invest 1998; 102:430–7.
20. Brown CK, Modzelewski RA, Johnson CS, et al. A novel approach for the identification of unique tumor vasculature binding peptides using

an E. coli peptide display library. Ann Surg Oncol 2000; 7:743–9.
21. Weller GE, Wong MK, Modzelewski RA, et al. Ultrasonic imaging of tumor angiogenesis using contrast microbubbles targeted via the tumor-binding peptide arginine-arginine-leucine. Cancer Res 2005; 65:533–9.
22. Henry DO, Chen SC, Wong MK, et al. Targeted molecular imaging of prostate cancer using tumor endothelium homing Arg-Arg-Leu peptides. J Clin Oncol 2006; 24:14582.
23. Yu MM, Wang RF, P Yan, et al. Design, synthesis and iodination of an Arg-Arg-Leu peptide for potential use as an imaging agent for human prostate carcinoma. J Label Compd Radiopharm 2008; 51:374–8.
24. Li S, Peck-Radosavljevic M, Koller E, et al. Characterization of $^{123}$I-vascular endothelial growth factor-binding sites expressed on human tumour cells: possible implication for tumour scintigraphy. Int J Cancer 2001; 91:789–96.
25. Hicklin DJ, Ellis LM. Role of the vascular endothelial growth factor pathway in tumor growth and angiogenesis. J Clin Oncol 2005; 23:1011–27.
26. Li S, Peck-Radosavljevic M, Kienast O, et al. Imaging gastrointestinal tumours using vascular endothelial growth factor-165 (VEGF165) receptor scintigraphy. Ann Oncol 2003; 14:1274–7.
27. Schaefer NG, Ma J, Huang P, et al. Radioimmunotherapy in non-Hodgkin lymphoma: opinions of U.S. medical oncologists and hematologists. J Nucl Med 2010; 51:987–94.
28. Carmeliet P, Jain RK. Angiogenesis in cancer and other diseases. Nature 2000; 407:249–57.